

## 7.4 EVOLUTION OF CONVECTIVE BOUNDARY LAYER IN DEEP VALLEY FOR AIR QUALITY MODELING

Charles Chemel\*, Jean-Pierre Chollet, Guillaume Brulfert and Eric Chaxel  
Laboratoire des Ecoulements Géophysiques et Industriels, UJF-CNRS-INPG, Grenoble, France

### ABSTRACT

Mixing depth structure and its evolution has been diagnosed from radar profiler data in the Chamonix valley (France) during summer 2003. The behaviour of  $C_n^2$  peaks coupled with the vertical air velocity variance  $\sigma_w^2$  were used to locate the height of the mixed layer. Tethersonde vertical profiles were carried out to investigate the lower layers of the atmosphere in the range of approximately 400-500 m a.g.l. High-resolution numerical simulations using the ARPS (Advanced Regional Prediction System) model have been performed with several grid nesting levels. Collected data in the Chamonix valley were used to evaluate the model results. The hierarchy of domains and models succeeds in reproducing realistic thermally driven processes in this deep narrow valley. Both ground surface and upper-levels calculated winds show good agreement with the observations.

### 1. INTRODUCTION

Alpine valley are particularly sensitive to air pollution due to emission sources generally concentrated close to the valley floor and local meteorology induced by complex terrain. The program POVA ('Pollution des Vallées Alpines') was launched in May 2000. The main objective of the POVA program is to characterize the pollution sources and study the relationship between atmosphere dynamics and pollution events in the Chamonix and Maurienne valleys (France). This study benefits from an exceptional context, with the 'Tunnel du Mont Blanc' (TMB) in the Chamonix valley being closed for nearly 3 years after a large accident in March 1999. The program includes several intensive field campaigns before and after the reopening of the TMB to heavy duty traffic, associated with 3D modeling.

Dynamical issues in mountainous areas has been discussed in numerous studies. Thermally driven winds in wide valleys are well documented, and Whiteman (1990) gives an overview of knowledge on the meteorological aspects. A stable nocturnal boundary layer forms at the surface at night when air temperature near the ground decreases in response to the radiational cooling of the surface. This process produces a shallow inversion and stable conditions, which reduces vertical mixing, thus confining surface-based pollutants to the lowest few hundred meters. Starting shortly after sunrise, the convective boundary layer (CBL) grows during the day due to surface heating. This process generates thermals which vertically mix heat, moisture, momentum, and pollutants.

During the POVA observation periods, the structure of the convective boundary layer was measured using a UHF radar profiler. Beside measuring winds, the radar profiler also measured reflectivity, which can be used to compute the refractive index structure parameter  $C_n^2$ . This parameter measures fluctuations in the refractive index of the atmosphere. The enhancement  $C_n^2$  often occurs where vertical gradients of virtual potential temperature  $\theta_v$  and mixing ratio  $r$  have their maximum values. The  $C_n^2$  can be a very useful parameter for estimating the CBL height. During the last decade, different  $C_n^2$ -based techniques have been investigated. White (1993) and Angevine *et al.* (1994) estimated CBL height in clear air using signal-to-noise ratio (SNR) peaks. Heo *et al.* (2003) have developed a method using both  $C_n^2$  peaks and vertical air velocity variance  $\sigma_w^2$ . This method is able to distinguish peaks due to the CBL height from peaks due to a cloud layer or a residual layer.

The turbulent dissipation rate  $\epsilon$  retrieval from spectral width measurements provides an additional information coupled reflectivity data. Jacoby-Koaly *et al.* (2002) give an excellent review of methods for  $\epsilon$  determination.

Due to ground clutter and atmospheric echoes, radar profilers are often blind close to the surface. Furthermore, for a reliable prediction of chemical species concentrations, mixing-height evolution during morning and evening transition periods is one essential parameter. Observational studies addressed this issue. Clements *et al.* (1989) investigated the mean properties of the nocturnal drainage flow down a valley using an instrumented tethered balloon and observed a strong down valley flow near the valley floor and a reversed up valley flow aloft. Whiteman (1982) looked into upward growth of the CBL during the morning transition in deep mountain valleys.

---

\* Corresponding author address: Charles Chemel, LEGI, BP 53 X, 38041 Grenoble, France; e-mail: [Charles.Chemel@hmg.inpg.fr](mailto:Charles.Chemel@hmg.inpg.fr).

During the last POVA field campaign in summer 2003, the lower layers of the atmosphere were documented using a small portable tethered balloon. Joined up with the wind profiler, the tethered balloon provided full vertical profiles.

The objective of the experiment was to catch the local mixing depth structure and its evolution in the Chamonix and Maurienne valleys. A peculiar emphasis was put on transition period to give a better understanding of the formation of the CBL.

Numerical simulations were compared with the POVA field data collected in winter and summer 2003. Large eddy simulation approach has been used to investigate local dynamics in both valleys. In the present paper, analyses and validation were performed for the last POVA field campaigns. This study will focus on the whole week of observation in the Chamonix valley during summer 2003. The ARPS (Advanced Regional Prediction System) model developed at the University of Oklahoma was used with several grid nesting levels. The Chamonix valley was finally resolved on a 93 E-W by 103 N-S grid with spacings of 300 m  $\times$  300 m in the horizontal directions. This grid encompassed a domain of about 25 km  $\times$  25 km. Results from ARPS were input afterwards in the meso-scale chemical-transport model TAPOM (Brulfert *et al.*, 2003).

## 2. OBSERVATIONAL SITE

The present study refers to a fraction of the French Alpine region. The topography of the region (Figure 1) is composed of various valleys of different shapes, lengths and orientation that makes the assessment of the air flow especially challenging. The Chamonix valley (site A) runs from southwest to northeast for about 15 km, is over 2000 m deep in average. The altitude of the highest mountain of the southeast mountain ridge (the Mont-Blanc) is 4810 m a.s.l. The peak-to-peak wavelength is about 4 km and the width of the valley bottom is about 1.5 km. The Maurienne valley (site B) is five times as long as the Chamonix valley. The length of the curved valley is about 80 km. The mountain ridges on both sides reach altitudes of around 3000 m a.s.l. and the width of the valley bottom is about 2 km. Both valleys have sidewalls with slopes of 40°-50°, and have a valley floor that falls in the range of approximately 13-14 m per km.

Radar profiler observation sites are indicated by the letters A and B in Figure 1. Site A is located near the Chamonix valley bottom at an altitude of 1040 m a.s.l. Site B is located close to the center of the Maurienne valley at an altitude of 1090 m a.s.l.

## 3. EXPERIMENTAL APPROACH

### 3.1. Equipment

The mobile wind profiler used in the POVA experiment is a 'clean-air' three panel 1238 MHz UHF Doppler radar system designed by Degreane Horizon to measure both wind speed and direction 24 hours a day under all weather conditions. 'Clean air' radars detect irregularities in backscat-

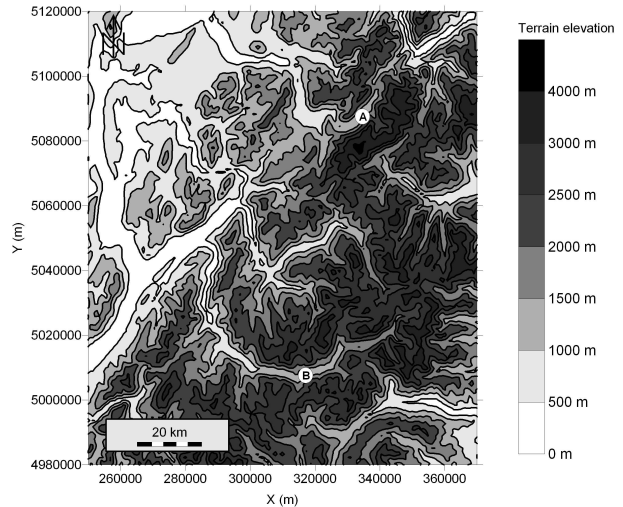


**Figure 1:** Overview of a part of the Alps with location of the ground based measurements (letter in circles) in UTM coordinate system, zone 32. Colours in the map indicate altitude (see attached colour scale)

tered signals due to refractive index inhomogeneities caused by turbulence. In the lower troposphere these inhomogeneities are mainly produced by humidity fluctuations. The Doppler shift associated with the turbulence provides a direct measurement of the mean radial velocity along the radar beam. To enable full wind vectors (zonal, meridional and vertical) to be calculated a set of measurements are made in three independent directions. The wind profiler consists of three panels to emit and receive three separate beams one vertical from the central panel and the other two at an elevation of 73° to enable full wind vectors to be calculated. Each panel is an array of eight aerial (antenna) every one being an assembly of eight collinear dipoles. It operates by transmitting electromagnetic energy into the atmosphere and measuring the strength and frequency of backscattered energy. The used mode sampled the boundary layer from 80 m to 3500 m a.g.l. in the vertical, using a 80 m resolution.

Small, portable, tethered balloon data collection system provided experimental data close to the surface. In addition, the cable car up to *le Plan de l'Aiguille* (2350 m a.s.l.) from Chamonix (1040 m a.s.l.) was equipped with a data logger to monitor pressure, temperature, relative humidity and ozone ( $O_3$ ).

### 3.2. Collection and processing of data

Data were collected from 25 June through July 12, 2003 during the last POVA field campaigns. This study will focus on the whole week of observation in the Chamonix valley from 5 through July 12, 2003. Precipitation event occurred on July 9, 2003, affecting the quality and the quantity of collected data.

Located at *le Clos de l'Ours* (A) and *Modane* (B), the UHF wind profiler was operated continuously during the entire campaign in order to observe mean and turbulent

clear air conditions in the lower atmospheric layer. Data were collected using a three-beam cycle acquired every 6 min. The first three moments were computed with the weighted contiguous spectral lines selected during the last 30 min. The 30-min consensus performs a temporal filter over the considered period removing or smoothing out spurious unwanted echoes.

Vertical tethered balloon soundings of meteorological variables and  $O_3$  in the range of approximately 400–500 m a.g.l. were conducted at *les Praz de Chamonix* (A) and *Modane* (B), in a quite broad expanse. Vertical sounding operations at each site consisted of deployment of a Tethersonde Meteorological Tower System (TMT)<sup>TM</sup> by Vaisala Inc. with electrochemical concentration cell ozone sonde (Model 4Z ECC- $O_3$ -Sonde)<sup>TM</sup> by EN-SCI Corporation beneath a 5-m<sup>3</sup> helium-filled balloon and were restricted to daylight hours to meet aircraft safety considerations. Tethersonde flights were intermittent at both sites due to strong winds that halted operations after midday.

### 3.3. Results and discussion

For this study, hourly mixing depths were estimated from  $C_n^2$  data during the day using an algorithm proposed by Heo *et al.* (2003).  $C_n^2$  data were combined with the variance of vertical air velocity  $\sigma_w^2$  to monitor the growth of the CBL during the transition periods. Assuming that heat flux decreases linearly with height from the surface to the top of CBL in a dry convective mixed layer, this method consists in determining the ‘zero flux level’. The heat flux is proportional to the standard deviation of the vertical velocity (Weill *et al.*, 1980)

$$\frac{\sigma_w^3}{z} \approx \alpha^{3/2} \frac{g}{\theta} \overline{w'\theta'_v},$$

where  $z$  represents height above ground level and  $\alpha$  a universal constant ( $\alpha = 1.4$ ). Therefore, the CBL height corresponds to the level where  $\sigma_w^3/z$  becomes null. The peak of  $C_n^2$  close to the zero flux level is taken as the CBL height.

Other techniques were used to provide further informations. Daytime dissipation rates are almost constant with height in the mixing layer (Kitchen *et al.*, 1983). Above the CBL top, the dissipation rate rapidly decreases to near zero.  $\epsilon$  vertical evolution is used to get a better estimate of the mixing depth coupled with information derived from reflectivity data.

Figure 2 illustrates the diurnal changes in the mixed layer structure for July 8, 2003. The upper limit of the mixed layer is plotted as white dots from  $C_n^2$  peaks and the variance of vertical air velocity  $\sigma_w^2$ . At night, the strong stability in the nocturnal boundary layer confines vertical mixing of momentum and surface-based pollutants to a shallow layer (i.e., 100 to 200 m thick) near the ground. After daybreak (0800 UTC), the ground surface warms up, resulting in the growth of the CBL. The CBL grows up to an afternoon depth of 1500 m a.s.l. By early evening (2000 UTC), the stable conditions associated with the nocturnal boundary layer formes.

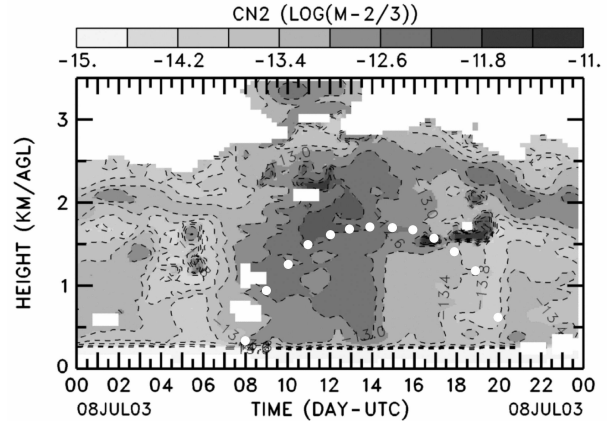


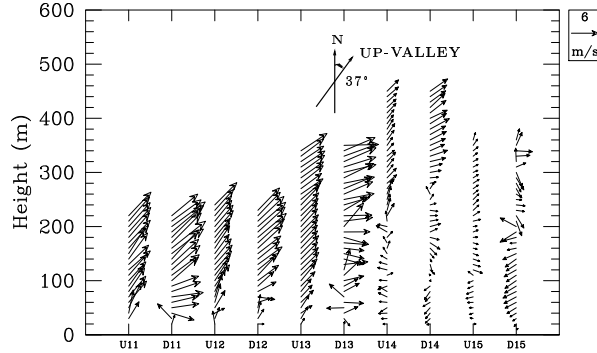
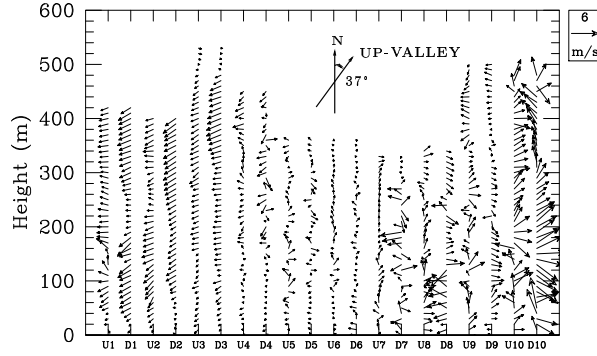
**Figure 2:** Time-height cross section of refractive index structure parameter  $C_n^2$  and the CBL heights (white dots) estimated by the maximum backscatter intensity method combined with the variance of vertical air velocity  $\sigma_w^2$  for July 8, 2003 at *le Clos de l’Ours* in the Chamonix valley

During morning and evening transition periods, wind structure pattern evolution,  $\theta_v$  and  $O_3$  profiles from tethered balloon measurements complement wind profiler data. Figure 3 shows wind structure pattern evolution from tethered balloon ascents and descents for July 8, 2003. Soundings show the reversal of the valley wind system during the transition periods. Wind direction reverses from down ( $50^\circ$ ) – to up ( $230^\circ$ ) in the morning (0900 UTC) and the opposite at night (2000 UTC). Wind speed culminates when being up-valley and peaks at 5 – 6 m/s at 1200 UTC.

## 4. NUMERICAL APPROACH

Large-eddy simulation was used to study meso-scale atmospheric flow fields in both valleys. Small scale modeling is required to take account of the whole frequency range of the fluid motions. The numerical simulations presented in this paper have been conducted with the Advanced Regional Prediction System (ARPS), version 4.5.2. Xue *et al.* (2000, 2001) give an extensive description of the code. Details on the ARPS formulation can also be found at <http://www.caps.ou.edu/ARPS>.

A generalized terrain following coordinate system is used in the ARPS model to solve the non-hydrostatic and compressible Navier-Stokes equation on a staggered Arakawa C-grid. The horizontal grid remains orthogonal while the vertical grid is stretched to follow the terrain, as in the sigma- $z$  coordinate system. A coordinate transformation is used to project the terrain-following coordinates to a regular grid in the computational space. The sound wave containing equations are integrated applying a split explicit time integration scheme to accommodate high-frequency acoustic waves. A leapfrog scheme is used to advance advection and diffusion at a large time step. The conservation equation for momentum, heat, mass, water substances, turbulent kinetic energy ( $TKE$ ) and the



#	Time (UTC)	#	Time (UTC)
1U	0634-0642	9U	1105-1114
1D	0642-0653	9D	1114-1125
2U	0653-0704	10U	1125-1133
2D	0704-0712	10D	1133-1148
3U	0745-0802		
3D	0802-0817		
4U	0817-0832	11U	1930-1936
4D	0832-0852	11D	1936-1941
5U	0852-0900	12U	1941-1946
5D	0900-0926	12D	1946-1959
6U	0926-0941	13U	1959-2010
6D	0941-0957	13D	2010-2057
7U	0957-1008	14U	2057-2109
7D	1008-1034	14D	2109-2126
8U	1034-1040	15U	2126-2133
8D	1040-1105	15D	2133-2141
U (Up)		D (Down)	

**Figure 3:** Wind structure pattern evolution. Tethered-balloon data, Chamonix valley, July 8, 2003

equation of moist air are solved. The vertical dynamic equation can be solved implicitly.

#### 4.1. Physiographic data and grid setup

A good representation of land surface characteristics is necessary for numerical models to reproduce realistically meteorological events and climatological patterns

(Marth, 2000). Particular atmospheric phenomena such as blocking of synoptic systems, valley winds and slope winds, can be generated or induced by the topography. The use of realistic and high-resolution topography is required to represent this surface feature. Similarly, the soil-vegetation characteristics are needful for the calculation of surface fluxes of heat, moisture, and momentum over rough surfaces.

Physiographic data sources are provided by Air de l'Ain et des Pays de Savoie (AAPS) and are available with a 100-meter resolution. Data contains orography, roughness, soil type and vegetation type.

The top and bottom boundaries are processed as rigid free-slip boundaries. Surface fluxes are parameterized to take into account the influence of the rough bottom surface. Land-surface energy budget is calculated by a simplified soil-vegetation model (Noilhan and Planton, 1989 ; Pleim and Xiu, 1995). Rayleigh damping was applied to the top one-third of the total domain depth (Xue *et al.*, 2000). Lateral boundary conditions were externally-forced. Lateral boundary values were obtained from the output of larger-scale simulations performed with the Fifth-Generation Penn State/NCAR Mesoscale Model (MM5) version 3 (Grell *et al.*, 1995). MM5 is a non-hydrostatic code which allows meteorological calculation at various scales on a staggered Arakawa B-grid with a two-way nesting technique. The vertical coordinate is a sigma- $p$  coordinate what is similar to a terrain following coordinate. In the present study three different domains were used as shown in Table 1.

Typical extent		
Domain 1	France (1500 km)	
Domain 2	Southeastern France (650 km)	
Domain 3	Savoie mountains (350 km)	
Mesh points		Grid size
$n_x$ E-W	$n_y$ N-S	$\Delta x = \Delta y$ (km)
Domain 1	45 × 51	27
Domain 2	69 × 63	9
Domain 3	96 × 96	3

**Table 1:** Mesh size and dimensions of MM5 domains used for simulations

Boundary conditions of domain 1 was driven by the European Centre for Medium-Range Weather Forecasts (ECMWF) gridded analyses available every 6 hours at 0Z, 6Z, 12Z and 18Z with a horizontal resolution of  $0.5^\circ$  and on 16 pressure levels from 1000 to 50 hPa. In addition the ECMWF first-guesses were used every 6 hours at 3Z, 9Z, 15Z and 21Z to obtain a better temporal description of the synoptic situation. Four Dimensional Variational Analysis (4D-Var) technique was used in the coarser domain to drive the perturbations needed to control the simulation results (Zou *et al.*, 1997).

Vertically MM5 uses 27 layers with thicknesses ranging from 65 m at the ground to 2 km. The top of the model is at the pressure 100 Pa. The planetary boundary layer

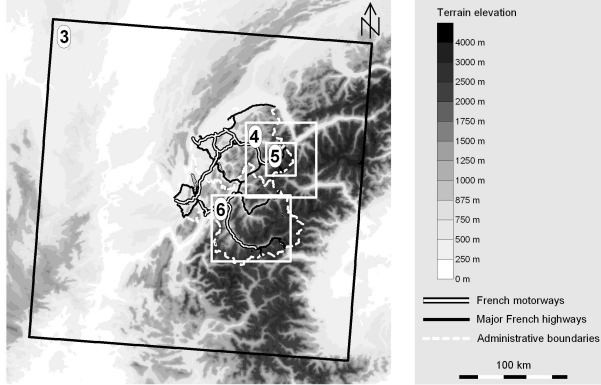


**Figure 4:** Geographical extents of ARPS domains used for simulations

(PBL) is described with about 15 layers from 0 to 2000 m a.g.l. with the non-local mixing MRF scheme described by Hong and Pan (1996).

External boundary meteorological fields from the third MM5 domain are applied to ARPS grids using one-way interactive nesting. ‘One-way’ means that the larger grid influences the smaller one, but not vice versa. A relaxation zone similar to that discussed by Davies (1976) was employed to smooth gradients near the lateral boundaries.

For the Chamonix valley modeling with ARPS, two grid nesting levels were used. The first domain is resolved on a 67 E-W by 71 N-S grid with a 1 km horizontal resolution. The grid was chosen to be a one-third reduction in horizontal grid spacing when compared to the third MM5 grid. This run was then further nested to the final fine grid. The Chamonix valley was resolved on a 93 E-W by 103 N-S grid with spacings of 300 m  $\times$  300 m in the horizontal directions. This grid encompassed a domain of about 25 km  $\times$  25 km. The computation was made on 30 layers. The vertical direction was stretched to accommodate approximately 30 m spacing near the lower wall.

The Maurienne valley was resolved on a 75 E-W by 63 N-S grid with a 1 km resolution. Only one domain is necessary. The lowest layer has a thickness of about 70 m.

Figure 4 and Table 2 give the spatial coverage and the resolution of the different grids used in the presented ARPS simulations.

#### 4.2. Numerical parameters

In the ARPS code, fourth-order horizontal and second-order quadratically conservative differencing scheme was used to solve the momentum and scalar advection terms. Time steps for advection  $\Delta t$  and acoustic modes  $\Delta \tau$  were determined using the Courant-Fredrichs-Levy (CFL) stability condition deduced from minimum vertical grid spacing and maximum velocity. Practical time step for the fine grid was  $\Delta t = 1$  s and  $\Delta \tau = 0.1$  s. For a typical run on the IBM SP Power4 ‘zahir’ of the Institut du Développement et des Ressources en Informatique Scientifique (IDRIS) on 8 processors with the fine 93  $\times$  103  $\times$  30 grid, the total

Typical extent		
Domain 4	Haute-Savoie Dept. (50 km)	
Domain 5	Chamonix valley (25 km)	
Domain 6	Maurienne valley (100 km)	
Mesh points		Grid size
$n_x$ E-W	$n_y$ N-S	$\Delta x = \Delta y$ (km)
Domain 4	67 $\times$ 71	1
Domain 5	93 $\times$ 103	0.3
Domain 6	75 $\times$ 63	1

**Table 2:** Mesh size and dimensions of ARPS domains used for simulations

CPU time per time step per grid point was  $9.40 \times 10^{-6}$ . The code achieved 41.6 Gflops for 8 processors and the memory requirement was a total of 81.6 MB.

The chosen treatment of convective boundary layer turbulence is a combination of the 3D level-1.5 Deardorff subgrid-scale (SGS) scheme and an 1D ensemble turbulence scheme of Sun and Chang (1986). This formulation accounts for the non-local PBL depth instead of the local vertical grid spacing inside an unstable layer to parametrize the local mixing due to SGS turbulence.

Moisture processes were included, but microphysics were disabled since only clear days were simulated. Informations on surface and deep soil temperature predicted by MM5 were used for initialization purpose. Simulation results were particularly sensitive to the surface and deep soil moisture. Their values are chosen so that valley characteristics are close to a typical Alpine valley. During relative dry periods in summer, the volumetric surface and deep soil moistures are about  $0.2 \text{ m}^3 \text{ m}^{-3}$  (Zappa *et al.*, 2000).

#### 4.3. Results and discussion

Numerical results from the model were compared to measurements for the whole week of observation in the Chamonix valley during summer 2003.

In figure 5, data from the model and *le Bois du Bouchet* monitoring station point out the agreement except on July 9, 2003, with clouds and precipitation which are not considered in the model. The spin up from initial condition is rather short (about 2 hours) which may be attributed to the appropriate nesting of boundaries by the models run at larger scales. The time evolution of wind force is well reproduced, amplitude is slightly overestimated which may be due to trees surrounding the station. In spite of rather low wind force values, direction is well predicted (beware of cyclic axis:  $0^\circ = 360^\circ$ ).

Wind direction and force from the wind profiler are compared to corresponding values computed in the model for the whole week of field campaign (see figure 6). The wind direction reverses twice a day from down to up valley in the morning and the opposite at night, and significantly differs from the synoptic wind at higher altitude. Wind shear allows to document the mixed layer thickness

and its evolution from a day to another. Particular features may be observed because of a weather perturbation on July 9, 2003.

Figures 7a and 7b show a valley cross-section plotted along the North direction through *le Clos de l'Ours* monitoring station. In figure 7a, isovalues of  $TKE$  as computed from the model at 1200 UTC on July 8, 2003 shows a turbulent activity which peaks at the top of the valley at about 2500 m a.s.l. as documented in detailed calculations of wind circulations in an ideal valley (Kerbioui, 2004). It comes from thermally driven vertical motions as demonstrated by figure 7b with the isovalues of the vertical velocity  $w$ . This picture is typical of a midday wind circulation when thermal activity is at its most. It emphasizes the rather small scales involved in the flow fields and associated mixing in such narrow valley.

The hodograph of figure 8 from the model in *Argentière* ground station behaves approximatively as a closed loop. It describes that the valley wind system reverses twice a day. It does not align along the valley direction, which suggests at least from 0800 to 1000 UTC and 1800 and 2200 UTC effects of vertical mixing or/and slope winds.

## 5. SUMMARY & CONCLUSIONS

Documentation of wind reversal and mixing height with wind profiler and tethered balloon data were performed during the last POVA field campaign in summer 2003. The  $C_n^2$  peaks corresponding to the CBL heights were in good agreement with the rawinsonde estimated CBL heights when vertical mixing owing to solar heating was significant and the vertical gradient of both  $\theta$  and  $r$  in the entrainment zone was strong. The tethered balloon-derived mixing heights were especially useful to study the reversal of the down-valley wind system during the morning transition. A fraction of the incoming radiation received on the valley unfolded surface is converted to sensible heat flux. Sensible heat flux generates the development of a CBL over the surface which grows up to an afternoon depth of 1500 m a.s.l. A quantization of the mixing and the vertical transport through the CBL is subject to future research.

Numerical simulations using ARPS were compared with the POVA field data collected during the whole week of field campaign in the Chamonix valley during summer 2003. The simulated meteorological fields are in good agreement with observations except on July 9, 2003 with storm conditions. The hierarchy of domains and models succeeds in reproducing realistic dynamical processes in this deep narrow valley. Local thermally driven wind circulation within the valley – up-valley flow during day and down-valley flow during night – was well simulated by the model. Flow fields computed from the model are passed to chemical-transport model in order to assess concentrations of pollutants.

*Acknowledgements.* The research has been supported by the Rhône-Alpes Region, the Agency for Environment and Energy Management (ADEME), the Ministry of Equipment, Transport and Housing (METL) and the Min-

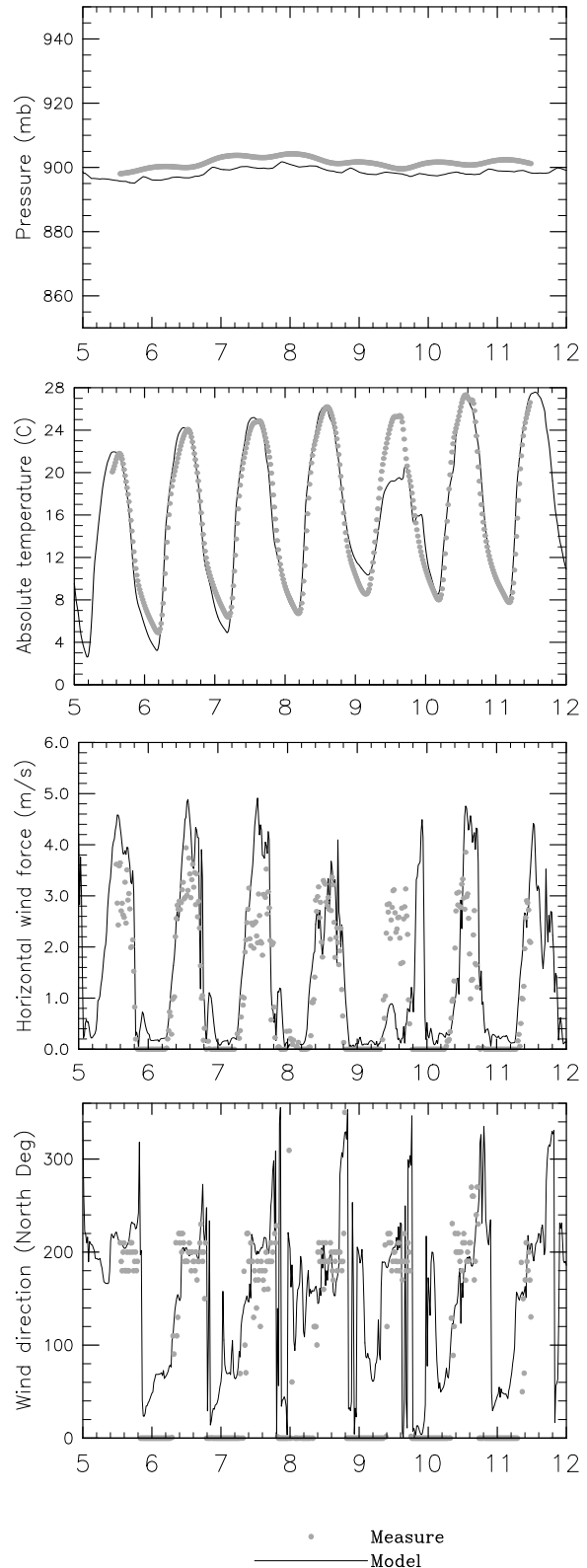


**Figure 5:** *Le Bois du Bouchet* monitoring station compared to model results for the whole week of field campaign during summer 2003 in the Chamonix valley

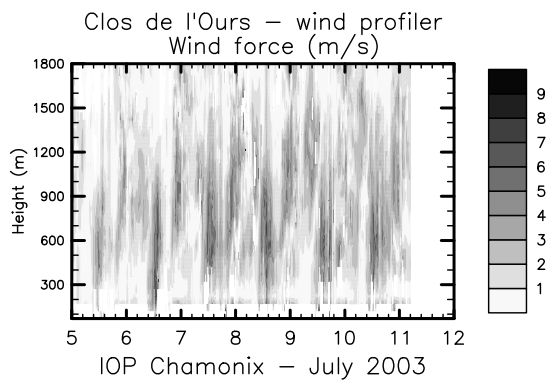
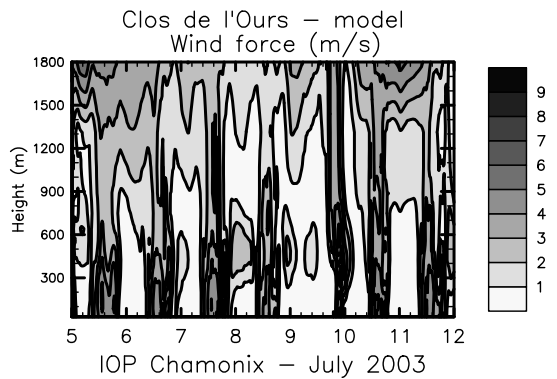
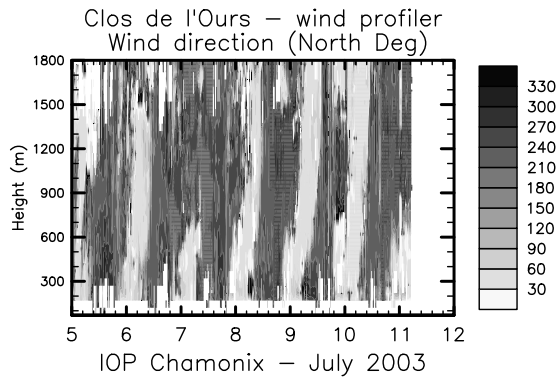
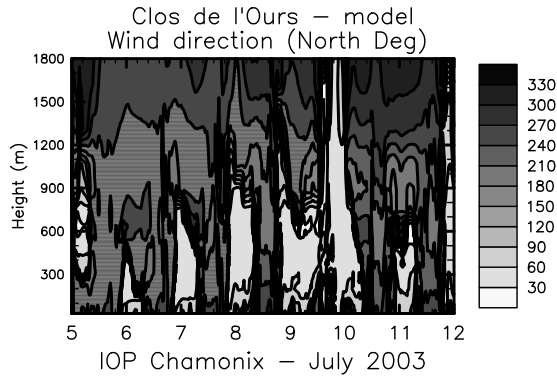


**Figure 6:** Wind structure pattern evolution from ARPS compared to measurements from the wind profiler for the whole week of field campaign during summer 2003 at *le Clos de l'Ours* in the Chamonix valley

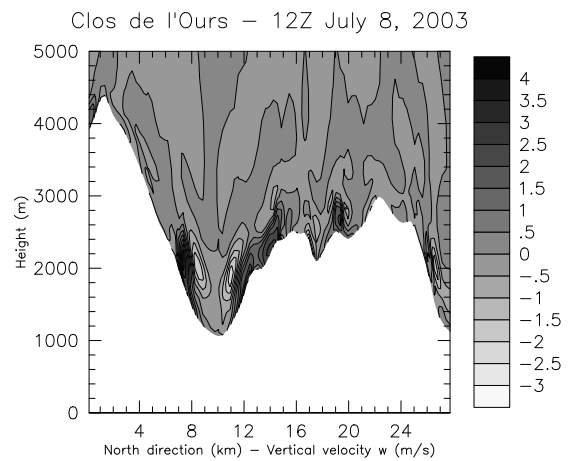
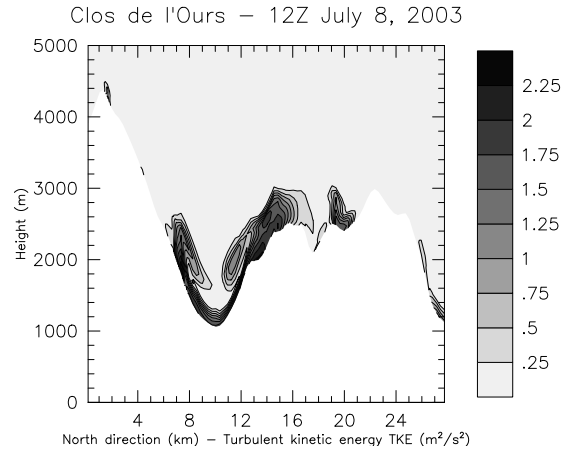


**Figure 7:** Valley cross-section along the North direction through *le Clos de l'Ours* monitoring station from the simulation at 1200 UTC on July 8, 2003. (a) Isovalues of TKE (b) Isovalues of  $w$

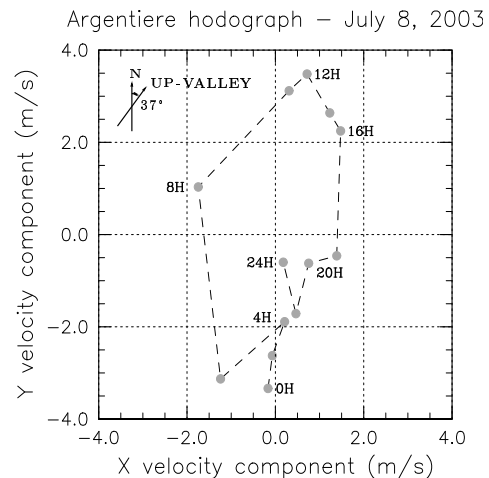


**Figure 8:** Hodograph from the model in *Argentiere* ground station on July 8, 2003

istry for Ecology and the Durable Development (MEDD). We are grateful to Rémi Dallmayr for assistance with tethered operations. We thank Bernard Campistron for providing us with a listing of his radar postprocessing tool. We also thank Bruno Bénech for a number of very helpful discussions on the tethered device.

## REFERENCES

- Angevine, W. M., A. B. White, and S. K. Avery, 1994: Boundary-layer depth and entrainment zone characterization with a boundary-layer profiler. *Boundary-Layer Meteorol.*, **68**, 375–385.
- Burlfert, G., E. Chaxel, C. Chemel, and J. P. Chollet: 2003, Numerical simulation of air quality in chamonix valley, use of different chemistry indicators. *Proc. of the 14th IUAPPA International Conference Air Quality – Assessment and policy at local, regional and global scales*, Dubrovnik, Croatia, 661–667.
- Clements, W. E., J. A. Archuleta, and D. E. Hoard, 1989: Mean structure of the nocturnal drainage flow in a deep valley. *J. Appl. Meteor.*, **28**, 457–462.
- Davies, H. C., 1976: A lateral boundary formulation for multi-level prediction models. *Quart. J. Roy. Met. Soc.*, **102**, 405–418.
- Grell, G. A., J. Dudhia, and D. R. Stauffer, 1995: A description of the fifth-generation penn state/ncar mesoscale model (mm5). NCAR Technical Note NCAR/TN-398+STR, NCAR, Boulder, CO, 117 pp.
- Heo, B. H., S. Jacoby-Koaly, K. E. Kim, B. Campistron, B. Bénech, and E. S. Sung, 2003: Use of the doppler spectral width to improve the estimation of the convective boundary layer height from uhf wind profiler observations. *J. Atmos. Oceanic Technol.*, **20**, 408–424.
- Hong, S. Y. and H. L. Pan, 1996: Nonlocal boundary layer vertical diffusion in a medium-range forecast model. *Mon. Weath. Rev.*, **124**, 2322–2339.
- Jacoby-Koaly, S., B. Campistron, S. Bernard, B. Bénech, F. Ardhuin-Girard, J. Dessens, E. Dupont, and B. Carissimo, 2002: Turbulent dissipation rate in the boundary layer via uhf wind profiler doppler spectral width measurements. *Boundary-Layer Meteorol.*, **103**, 361–389.
- Kerbiriou, M. A., 2004: *Dynamique d'une inversion thermique, transport et mélange en vallée encaissée: une étude numérique tridimensionnelle*. Thèse, spécialité mécanique des milieux géophysiques et environnement, Université Joseph Fourier, France.
- Kitchen, M., J. R. Leighton, and S. J. Caughey, 1983: Three case studies of shallow convection using a tethered balloon. *Boundary-Layer Meteorol.*, **27**, 281–308.
- Marth, L., 2000: Surface heterogeneity and vertical structure of the boundary layer. *Boundary-Layer Meteorol.*, **96**, 33–62.
- Noilhan, J. and S. Planton, 1989: A simple parametrization of land surface processes for meteorological models. *Mon. Weath. Rev.*, **117**, 536–549.
- Pleim, J. E. and A. Xiu, 1995: Development and testing of a surface flux and planetary boundary layer model for application in mesoscale models. *J. Appl. Meteor.*, **34**, 16–32.
- Sun, W. Y. and C. Z. Chang, 1986: Diffusion model for a convective layer. part i: Numerical simulation of convective boundary layer. *J. Climate Appl. Meteor.*, **25**, 1445–1453.
- Weill, A., C. Klapisz, B. Strauss, F. Baudin, C. Jaupart, P. van Grunderbeck, and J. P. Goutorbe, 1980: Measuring heat flux and structure functions of temperature fluctuations with an acoustic doppler sodar. *J. Appl. Meteor.*, **19**, 199–205.
- White, A. B.: 1993, Mixing depth detection using 915-mhz radar reflectivity data. *Proc. of the 8th Symp. on Meteorological Observations and Instrumentation*, Anaheim, CA, Amer. Meteor. Soc., 248–250.
- Whiteman, C. D., 1982: Breakup of temperature inversions in deep mountain valleys: Part i. observations. *J. Appl. Meteor.*, **21**, 270–289.
- Whiteman, C. D.: 1990, *Observations of thermally developed wind systems in mountainous terrain*, Amer. Meteor. Soc., Boston, MA, chapter 2 in *Atmospheric processes over complex terrain*, W. Blumen Ed., Meteorological Monographs, **23**, no. 45. 5–42.
- Xue, M., K. K. Droegemeier, and V. Wong, 2000: The advanced regional prediction system (arps) – a multi-scale non hydrostatic atmospheric simulation and prediction model. part i: Model dynamics and verification. *Met. Atm. Phys.*, **75**, 161–193.
- Xue, M., K. K. Droegemeier, V. Wong, A. Shapiro, K. Brewster, F. Carr, D. Weber, Y. Liu, and D. Wang, 2001: The advanced regional prediction system (arps) – a multi-scale non hydrostatic atmospheric simulation and prediction tool. part ii: Model physics and applications. *Met. Atm. Phys.*, **76**, 143–165.
- Zappa, M., N. Matzinger, and J. Gurtz, 2000: Mesoscale alpine programme (map) hydrological and meteorological measurements at claro (ch) – lago maggiore target area. Technical Report 10(2), Dept. of Civil Engineering, Univ. of Brescia, Italy, 35 pp.
- Zou, X., F. Vandenberghe, M. Pondeva, and Y. H. Kuo, 1997: Introduction to adjoint techniques and the mm5 adjoint modeling system. NCAR Technical Note NCAR/TN-435+STR, NCAR, Boulder, CO, 110 pp.